UCLA
UCLA Previously Published Works

Title

Diborane Interactions with Pt7/Alumina: Preparation of Size-Controlled Borated Pt Model Catalysts

Permalink

https://escholarship.org/uc/item/6nc4s740

Journal

The Journal of Physical Chemistry C, 122(3)

ISSN

1932-7447

Authors

Baxter, Eric T
Ha, Mai-Anh
Cass, Ashley C
et al.

Publication Date

2018-01-25

DOI

10.1021/acs.jpcc.7b10423

Peer reviewed

eScholarship.org Powered by the California Digital Library
University of California

Diborane Interactions with Pt_7/alumina: Preparation of Size-Controlled Borated Pt Model Catalysts with Improved Coking Resistance

Eric T. Baxter,[†] *Mai-Anh Ha*,[‡] *Ashley C. Cass*, [†] *Huanchen Zhai*,[‡] *Anastassia N. Alexandrova,*[‡,§,*] *and Scott L. Anderson*[†,*]

[†] Department of Chemistry, University of Utah,

[‡] Department of Chemistry & Biochemistry, University of California, Los Angeles,

[§] California NanoSystems Institute, Los Angeles, CA 90095.

Abstract

Bimetallic catalysts provide the ability to tune catalytic activity, selectivity, and stability. Model catalysts with size-selected bimetallic clusters on well-defined supports offer a useful platform for studying catalytic mechanisms, however, producing size-selected bimetallic clusters can be challenging. In this study, we present a way to prepare bimetallic model (Pt_nB_m/alumina) cluster catalysts by depositing size-selected Pt_7 clusters on an alumina thin film, then selectively adding boron by exposure to diborane and heating. The interactions between Pt_7/alumina and diborane were probed using temperature-programmed desorption/reaction (TPD/R), X-ray photoelectron spectroscopy (XPS), low energy ion scattering (ISS), plane wave density functional theory (PW-DFT), and molecular dynamic (MD) simulations. It was found that the diborane exposure/heating process does result in preferential binding of B in association with the Pt clusters. Borated Pt clusters are of interest because they are known to exhibit reduced affinity to carbon deposition

in catalytic dehydrogenation. At high temperatures, theory, in agreement with experiment, shows that boron tends to migrate to sites beneath the Pt clusters forming Pt-B-O_{suf} bonds that anchor the clusters to the alumina support.

I. Introduction

Carbon deposition (i.e. “coking”) leads to deactivation of catalysts in important reactions such as Fisher-Tropsch synthesis,[1] hydrocarbon cracking,[2] and alkene dehydrogenation.[3] It has been demonstrated that boration of extended surfaces of Co[4] and Ni[5] can extend the lifetime of catalysts without compromising their activity toward Fischer-Tropsch synthesis and steam reforming, respectively. In both processes, coking is the mechanism of deactivation. We recently showed that boration also reduces coking on size-selected Pt clusters deposited on alumina during dehydrogenation of alkenes.[6] This type of catalytic system is novel and so-far largely under-investigated, including several aspects of their preparation, experimental characterization, theoretical analysis, and structural, dynamical, and chemical properties.

Model catalysts with atomically size-selected clusters on well characterized supports provide a useful platform for studying catalysis mechanisms, allowing independent control of the size and density of catalytic sites, and facilitating detailed theoretical studies. Bimetallic catalysts provide important opportunities to tune catalytic activity, selectivity, and stability. However, extending the size-selected model catalyst approach to bimetallic clusters is challenging. One approach is to use alloy or dual target cluster sources that directly produce bimetallic clusters in the gas phase, which can then be mass selected and deposited to create bimetallic model catalysts.[7-10] This approach is quite general, in principle, however, for several reasons it becomes increasingly difficult as the cluster size increases. The cluster source intensity is “diluted” over an increasing number of possible M_xN_y combinations, and the intensity is further decreased by the need for high mass-selector resolution to separate closely-spaced masses. Intensity is

important, because clusters quickly become contaminated due to substrate-mediated adsorption,[11-13] even in ultra-high vacuum (UHV). In many cases, natural isotope distributions exacerbate these problems such that clean selection of both size and composition may be impossible except for very small clusters. For example, Pt has *major* isotopes with atomic masses 194, 195, 196, and 198, and boron has isotopes with atomic masses 10 and 11. Thus, even for clusters containing only three Pt atoms, the width of the Pt isotopologue distribution is greater than the boron mass, resulting in mass overlaps between Pt_3B_n and $Pt_3B_{n\pm1}$.

One motivation for this paper is to report a complementary approach to producing size-selected bimetallic cluster catalysts, in which mass-selected cluster deposition is used to create a size-selected model catalyst (here, Pt_n/alumina), which is then used to seed deposition of a second element to create a bimetallic model catalyst (here, Pt_nB_m/alumina). The challenge is to find conditions where boron deposits only on the Pt clusters, and then to characterize the nature of the resulting doped clusters.

II. Methods

As outlined below, alumina-supported size-selected $Pt_{4,7,8}$ model catalysts were prepared, and then exposed to diborane and heated to drive decomposition and H_2 desorption. The goal is to selectively borate the Pt clusters, thus it is important to understand how diborane interacts with both Pt_n clusters and the alumina support. These interactions were probed by temperature-programmed desorption and reaction (TPD/R), low energy He^+ ion scattering (ISS), and X-ray photoelectron spectroscopy (XPS) experiments on both Pt-free alumina and Pt_n/alumina samples, by plane wave density functional theory (PW-DFT) calculations of adsorption geometries and energetics, and molecular dynamic (MD) simulations

of borane surface chemistry. We previously showed that the chemical consequences of boration are similar for different Pt cluster sizes.[6] Here we focus on the boration mechanism, using Pt_7/alumina as the example system.

A. Computational: As discussed previously in detail,[14] PW-DFT calculations with projector augmented wave potentials[15-16] and the PBE[17] functional were implemented in the Vienna Ab initio Simulation Package (VASP).[18-21] The bulk-optimized unit cell with lattice constants of a = 4.807 Å and c = 13.126 Å was grown to a (3 × 3) surface, a slight expansion as compared to experiment.[22-23] A vacuum gap of 15 Å was added to the slab. The bottom half of the surface was kept fixed. For all calculations, convergence criteria of 10^{-5} (10^{-6}) eV for geometric (electronic) relaxations, expansion of the plane waves' kinetic energy to 400.0 eV, and a k-point grid of 1 × 1 × 1 centered at the Γ-point were instituted. We previously discussed the global optimization of Pt_7 on the model α-alumina surface,[14] finding a number of low-lying isomers for Pt_7/alumina. As shown below, the global minimum has Pt_7 in a prismatic (i.e., 3D) structure with Pt_7-alumina adsorption energy of -5.09 eV, however, there are isomers only 0.05 eV higher in energy in which all Pt atoms are in a single layer bound to the alumina surface.

A *per manum* search for diborane adsorption geometries associated with both the prismatic and single layer Pt_7/alumina structures was made, starting with the molecule positioned at bridging, hollow, and atomic (atop) sites, oriented both parallel and normal to the surface plane, and rotated in various orientations. The starting geometries focused on adsorption of diborane to the Pt clusters, rather than to the α-Al_2O_3 surface. The adsorption energy of diborane was calculated via the relation:

$$E_{B2H6} = E[\text{Surf} + Pt_7\text{-}B_2H_6] - E[B_2H_6]_{gas} - E[\text{Surf} + Pt_{7,glob}].$$

Ab-initio MD calculations, starting at the lowest minimum of diborane adsorbed on both the prismatic and single-layer Pt_7/alumina structures, were also performed. Equilibration of the system utilized the Nose-Hoover thermostat and an electronic convergence criterion of 10^{-8} eV per 1 fs time-step was implemented. The global optimization of Pt_4B_4 adsorbed on alumina was performed using the Basin Hopping method adapted for surface deposited clusters.[24] The local minima search for gas phase Pt_4B_4 also utilized Basin Hopping. The adsorption energy of Pt_4B_4 was taken as

$$E_{ads} = E[Surf + Pt_4B_4] - E[Pt_4B_4]_{gas,glob} - E[Surf].$$

B. Experimental: The experiments were conducted with an instrument consisting of a mass-selected metal cluster ion deposition beamline[25] that terminates in an ultrahigh vacuum (~1.5×10^{-10} Torr) analysis chamber that allows *in situ* sample preparation and characterization, as discussed previously, along with several of the experimental protocols used here.[12, 26-27] The Pt_n/alumina model catalysts were prepared on a 7×7 mm Ta(110) single crystal mounted using Ta heating wires to a liquid nitrogen reservoir at the end of a manipulator. The sample temperature was controlled between 110 and >2100 K by the combination of resistive and electron-bombardment heating and liquid nitrogen cooling. Temperature was measured by a C-type thermocouple spot welded to the back of the Ta single crystal.

Procedures for alumina film growth were adapted from the Goodman[28-30] and Madey[31-32] groups. At the beginning of each experiment, the Ta single crystal was annealed above 2100 K for 5 minutes or until no surface contaminants were detected by XPS and ISS. For alumina film growth, the Ta(110) substrate was transferred to a separately pumped UHV antechamber, heated to 970 K in 5×10^{-6} Torr of O_2, while exposed to Al evaporating from a crucible mounted normal to the

Ta(110) surface. In previous studies, we demonstrated that the reactivity, adsorbate binding, and electronic properties of Pd clusters deposited on alumina were independent of film thickness in the 3-10 nm range. For these studies the typical growth rate was ~0.2 nm/min and 3-6 nm thick films were used.

Before beginning cluster deposition, the alumina/Ta(110) support was flashed to ~800 K to desorb adventitious adsorbates. To minimize the time the clusters were exposed to background gases, Pt cluster deposition was done as the sample cooled after the flash, beginning when the sample reached ~300 K. The clusters were deposited onto the alumina support through a 2 mm diameter mask, and cluster coverage was controlled by monitoring the neutralization current of soft landed (~1 eV/atom) clusters on the support. Unless stated otherwise, all samples were prepared with Pt_7 coverage of 2.14 x 10^{13} clusters/cm^2, amounting to 1.5×10^{14} Pt atoms/cm^2, equivalent to ~10% of a close-packed Pt monolayer.

TPD/R measurements were made using a differentially pumped mass spectrometer that views the main UHV chamber through the ~2.5 mm diameter aperture in a skimmer cone. The cone was surrounded by four directional dose tubes that pointed at the sample position, and gas doses for both TPD/R and diborane exposure were done using the tubes to minimize gas exposures to the vacuum system. To calibrate the exposures, we compared sub-saturation CO TPD signals for CO delivered through the dose tubes and through a gas inlet remote from the sample position. During both gas dosing and the subsequent TPD/R heat ramp, the chamber pressure was monitored by a nude ion gauge, and ion signals of interest were measured by the differentially pumped mass spectrometer. Diborane TPD/R was done by exposing samples to B_2H_6 at 130 K sample temperature, followed by heating to 700 K. For ethylene TPD/R, the sample was exposed to 5 L of

C_2D_4 at a sample temperature of 150 K (to minimize multilayer adsorption), cooled to 130 K, and then heated to 700 K while monitoring signals for $C_2D_4^+$, D_2^+, and various background gases.

Boron was introduced into the UHV system in the form of a diborane/argon gas mixture that we characterized mass spectrometrically to have actual composition of 4.8% diborane, 85% argon, and 10.2% H_2, the latter assumed to result from diborane decomposition during storage.[33] Diborane exposures were calculated based on the measured diborane mole fraction. In most experiments, boration was done by exposing the samples to 1.5 L of diborane at a sample temperature of 130 K, followed by heating to 700 K, which was found to be sufficient to drive desorption to completion. Note that 1.5 L diborane exposure corresponds to ~5.8 x 10^{14} diborane molecules impinging *per* cm^2, i.e., smaller than the total number of surface atoms, but almost four times larger than the number of Pt atoms. A few experiments were performed using a 0.5 L diborane exposure, where the number of impinging diborane molecules (1.9 x $10^{14}/cm^2$) was only ~25% greater than the number of Pt atoms present. The dose variation had little effect on the sample properties, suggesting that 1.5 L should be more than sufficient to saturate the Pt cluster binding sites.

Because the gas mixture contained hydrogen, and diborane decomposition also produces hydrogen, we studied TPD following pure D_2 exposure, in separate experiments. H_2 desorption during diborane TPD/R could not be monitored because the mass 2 background in the mass spectrometer was too high.

XPS (Al Kα) was used to examine both alumina and Pt_7/alumina samples after B_2H_6 exposure, both while holding the sample at the 130 K dose temperature, and after heating the sample to 700 K. Since both boron and Pt are present only in the

surface layer, and we know the Pt coverage quite precisely, the boron coverage was estimated from the ratio of B 1s and Pt 4d XPS integrated intensities. The Pt 4d XPS signal was used because of overlap between Pt 4f and Al 2p. Both Pt and B are present at low coverage, and because the B 1s photoemission cross section is ~40 times smaller than that for Pt 4d,[34] the boron XPS signal is quite weak. To improve the signal/noise, the boron XPS measurements were done using samples with double the normal Pt_n coverage (i.e., 0.2 ML). Higher cluster coverage undoubtedly resulted in some increase in cluster agglomeration during deposition and heating, however, because the effects of boration do not appear to be very dependent on cluster size,[6] a modest degree of agglomeration is unlikely to have a significant effect on the B/Pt ratio. To insure that the diborane exposure was sufficient to saturate the larger number of Pt_7 present, we also doubled the diborane dose to 3.0 L.

For ISS, a beam of 1 keV He^+ was loosely focused onto the surface at 45° angle of incidence and the energy distribution of He^+ scattered along the surface normal was measured. Peaks in ISS result from scattering of He^+ from single atoms in the sample, predominantly in the surface layer.[35] Multiple scattering and scattering from sub-surface layers contributes primarily to a weak background. In these experiments, ISS was used to monitor the intensities associated with Pt, Al, and O atoms in the top sample layer. H is undetectable by ISS, and the boron ISS signal also proved to be undetectable, due to the combination of low He^+ scattering cross section ($\sigma_{scatt} \propto Z_{target}$), low boron coverage, and rising background in that energy range from multiple scattering. Because ISS is a destructive technique, the ISS experiments were done either on separately prepared samples or at the end of other experimental sequences.

III. Results

A. Temperature programmed desorption/reaction following adsorption of B_2H_6 and D_2:

TPD/R experiments were used to identify species desorbing from alumina and Pt_7/alumina surfaces, and the associated temperature dependences (i.e. energetics). Because the literature shows that diborane can polymerize on surfaces,[36] we monitored masses relevant to known boranes of various sizes. Figure S1 in the supporting information shows the raw TPD signals for ion masses 11, 26, 48, and 59, which are low background masses corresponding to $B_1H_x^+$,$B_2H_x^+$, $B_4H_x^+$, and $B_5H_x^+$ (the ^{11}B:^{10}B isotope ratio is ~80:20). Figure 1 shows the data corrected,

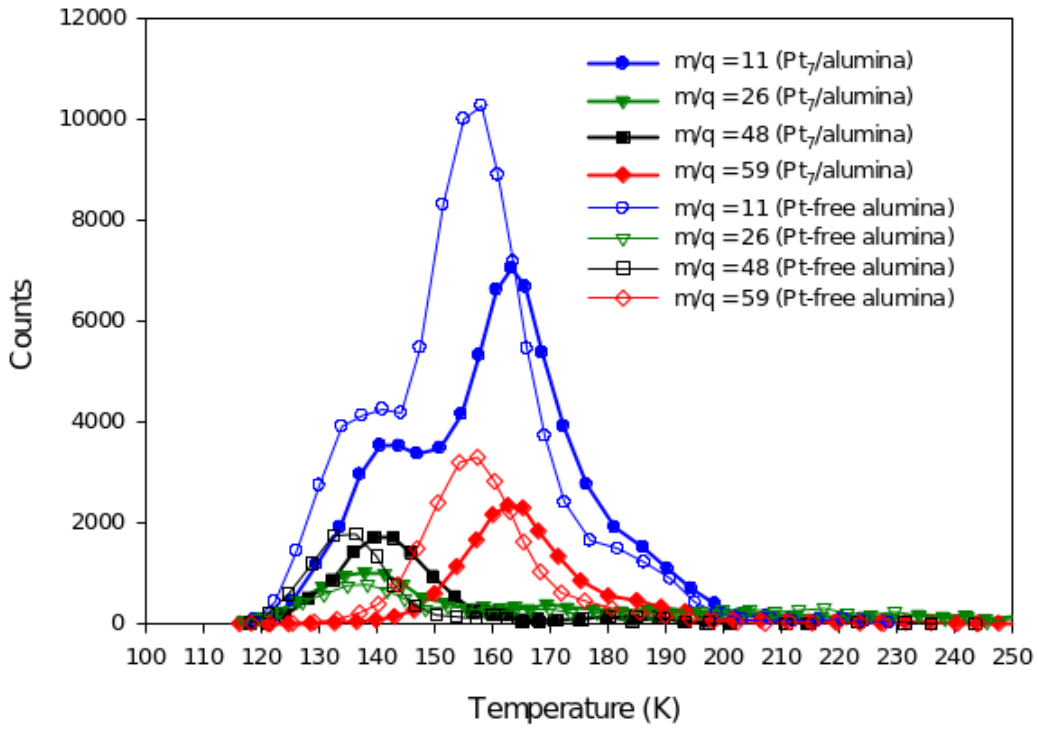

Figure 1. TPD spectra for select ion signals, corrected for EI cracking of borane species. Alumina and Pt_7/alumina samples were exposed to 1.5 L of diborane at 130 K, then heated at 3 K/sec while monitoring desorption mass

as described below, for the estimated contributions from fragmentation of higher boranes during election impact ionization (EI). Data are shown for desorption from both alumina and Pt_7/alumina samples, each exposed to 1.5 L of B_2H_6 at 130 K, then heated at 3 K/sec. Note that desorption starts at ~120 K, i.e., slightly below the dose temperature. This reflects the fact that diborane pumps out of the system slowly, so that there was a small additional exposure as the sample cooled to the TPD/R start temperature.

The assignment of the ion signals to desorbing species is complicated by the fact that boranes fragment extensively in EI.[37] We corrected the TPD signals for fragmentation of diborane, tetraborane (B_4H_{10}) and pentaborane (B_5H_9), which all have tabulated standard EI mass spectra, but did not attempt to correct for possible contributions from higher boranes (i.e., B_nH_m, $n > 5$). The dominant EI fragment ions for boranes tend to preserve the number of boron atoms ($B_nH_m \rightarrow B_nH_{m-x}^+$), however, there is some signal for essentially all possible $B_xH_y^+$ ($x \leq n$, $y \leq m$) fragments.[37] For example, mass 59 is the strongest peak in the EI mass spectrum of pentaborane (MW = 63.13), and mass 48 is the strongest peak for tetraborane (MW = 53.32), however, pentaborane EI also produces mass 48 with ~18% of the mass 59 intensity. Mass 26 is the most intense peak in the EI mass spectrum of diborane (MW=27.67), but 26 is also produced at the few percent level by EI of tetra- and pentaborane.

In Figure 1, no correction was made to the mass 59 intensity for possible contributions from EI of B_nH_m ($n \geq 6$), but the mass 48 signal was corrected for cracking of pentaborane, the mass 26 signal was corrected for cracking of pentaborane and tetraborane, and the mass 11 signal was corrected for contributions from penta-, tetra-, and diborane, using NIST standard mass spectra.[37]

As can be seen by comparing Figures 1 and S1, the corrections are generally quite small. The only qualitatively obvious change is that a peak in the raw signal for mass 48 in the 150 – 170 K range is shown to result almost entirely from EI cracking of pentaborane.

One surprise is that the mass 11 signal ($^{11}B^+$ and $^{10}BH^+$) is quite high, even after subtraction of the expected contributions from EI fragmentation of di-, tetra-, and pentaborane. We considered the possibility that the high mass 11 intensity might be an artifact of high mass spectrometer sensitivity to light masses, but this explanation is ruled out by the excellent agreement of our mass spectrum for diborane with the NIST standard diborane spectrum.[37] For example, when we leak diborane into our UHV system, we measure a mass 11 : 26 intensity ratio of ~0.3 : 1, in good agreement with the 0.28 : 1 ratio reported in the NIST database. It is also unlikely that the high mass 11 signal could result from EI fragmentation of higher boranes (B_nH_m, $n \geq 6$), because these, if present in high enough yield to account for such high mass 11 signal, would also result in much higher mass 59 signal than is observed. For example, hexaborane (B_6H_{10}) fragments in EI to produce both masses 11 and 59, however, the mass 59 intensity is ~1.5 times that of mass 11.[37]

Therefore, we conclude that the high mass 11 signal must largely result from desorption of some BH_x species, such as borane (BH_3). Diborane is a hydrogen-bridge-bonded dimer, with gas-phase dissociation enthalpy to 2 BH_3 of only 1.78 eV (i.e. 0.89 eV/BH_3),[38] and both BH_3 and BH_2 are detected mass spectrometrically in gas-phase pyrolysis of diborane at 300 °C.[39] We observe mass 11 desorption signal at low temperatures, raising the question of how BH_2 or BH_3 production is energetically feasible. For reactions of diborane on a surface, the energy required

to generate gas-phase BH_x may be supplied by recombination reactions (e.g. producing tetra- and pentaborane) or by formation of strong B-surface bonds.

We also looked for possible desorption of diborane surface reaction products during the 130 K dose, by monitoring masses 11, 26, 48, and 59 during diborane dosing. Signals for masses 11 and 26 were observed in a 0.27:1 ratio, as expected for gas phase diborane, indicating that the diborane sticking probability at 130 K is less than unity, and that little or no borane (BH_3) desorbs during the dose. Sub-unit sticking probability is unsurprising, given that 130 K is only 10 K below the peak of the diborane desorption during TPD/R. Small signals were also observed for masses 48 and 59 during the dose, but these were only 1.2 % and 0.4 % of the mass 26 (diborane) signal for the alumina sample and just 0.2 % and 0.1 % of the diborane signal for Pt_7/alumina. Clearly, if borane, tetraborane, or pentaborane form on the surface during the diborane dose, they mostly remain adsorbed until the sample is heated.

We estimated desorption energies for the different species by fitting the TPD/R temperature dependence to a second order kinetic model, i.e., assuming that the rate-limiting step is recombination of adsorbed B_xH_y fragments to generate the various boranes observed. The desorption energy distributions are shown in Figures S2 and S3, and the desorption energies all fall in the 0.4 to 0.5 eV range.

Diborane surface chemistry will be discussed in more detail after the rest of the experimental and theoretical results are presented. The most important points to keep in mind are:

1. Because all boranes fragment in EI to produce at least some mass 11, the absence of mass 11 signal above ~200 K implies that desorption of boron-containing species is complete by 200 K.

2. The mass 11 signal is far too large to be explained by EI fragmentation of B_nH_m ($n \geq 2$), implying that there is considerable desorption of BH_x.

3. The fact that masses 11, 48, and 59 are observed with higher intensities than mass 26 implies that most of the desorbing boron fraction is in the form of reaction products, rather than diborane.

4. Desorption from alumina and Pt_7/alumina are qualitatively similar, as might be expected, considering that 90% of the Pt_7/alumina surface is alumina.

5. The total amount of B_nH_m desorption is ~13% lower when Pt_7 is present at 10% coverage, and the desorption peaks are shifted 5 to 10 K to higher temperatures.

Species such as B_4H_{10} and B_5H_9 have the H:B ratios that are smaller than that for diborane (3:1). In addition, the XPS results discussed next show that a significant amount of boron remains on the surface after B_nH_m desorption has gone to completion. It is clear, therefore, that hydrogen must also be desorbing during diborane TPD/R. Observation of the diborane → H_2 desorption channel is not possible, both because the mass 2 background is high, and because the diborane reactant gas mixture has substantial H_2 concentration. To provide some insight into the binding/desorption behavior of hydrogen on Pt_7/alumina, we measured D_2 desorption from a separate Pt_7/alumina sample dosed with 5 L of D_2 at 130 K, and the result is shown in Figure S5. A small amount of D_2 desorption is observed in the temperature range below ~200 K, where borane desorption occurs, but ~90% of hydrogen desorption occurs at higher temperatures, between 200 and 400 K.

B. X-ray photoelectron spectroscopy: TPD/R probes the B_nH_m species that desorb upon heating, but from the perspective of selectively borating the Pt clusters, it is more important to understand the fate of the boron that remains on the surface. XPS was used to probe the fraction of B on the samples before and

after heating. Figure 2 compares B 1s spectra for both alumina and Pt_7/alumina samples, after exposure to 3 L of B_2H_6 at 130 K and after subsequent heating to 700 K. As noted above, the low B 1s photoemission cross section results in poor signal, and the XPS experiments were done using a sample with Pt_7 deposited at twice the normal coverage (~3 x 10^{14} Pt atoms/cm^2).

The B 1s XP spectrum of diborane adsorbed at 130 K on Pt_7/alumina is noisy (bottom right frame) but clearly indicates the presence of two components, fit by peaks at 189.7 and 193.9 eV, suggesting the presence of at least two boron chemical environments. The 130 K spectrum for Pt-free alumina (bottom left) has similar intensity peaking near 193 eV, but the low binding energy intensity is weaker than in the Pt_7/alumina sample. A similar two-component fit was used for this spectrum, resulting in peaks centered at 189.7 and 193.1 eV. After heating to 700 K, only a single broad B 1s feature remains for both alumina and Pt_7/alumina, peaking at 190.5 eV binding energy.

The integrated intensities, indicated in each frame of the figure, provide additional insight into diborane interactions with alumina and Pt_7. Note that the integrated B 1s intensity at 130 K, i.e., the total amount of boron adsorbed, is ~45% higher when Pt_7 is present. Heating to 700 K to desorb all volatile boron species, leads to loss of ~34% of the initial B 1s signal for alumina, but only ~22% of the (initially larger) B 1s signal for Pt_7/alumina. Thus, after heating, the amount of boron remaining on the sample is ~71% higher when Pt_7 is present, even though the Pt_7 coverage was only ~20%. This result can be compared to the TPD/R results,

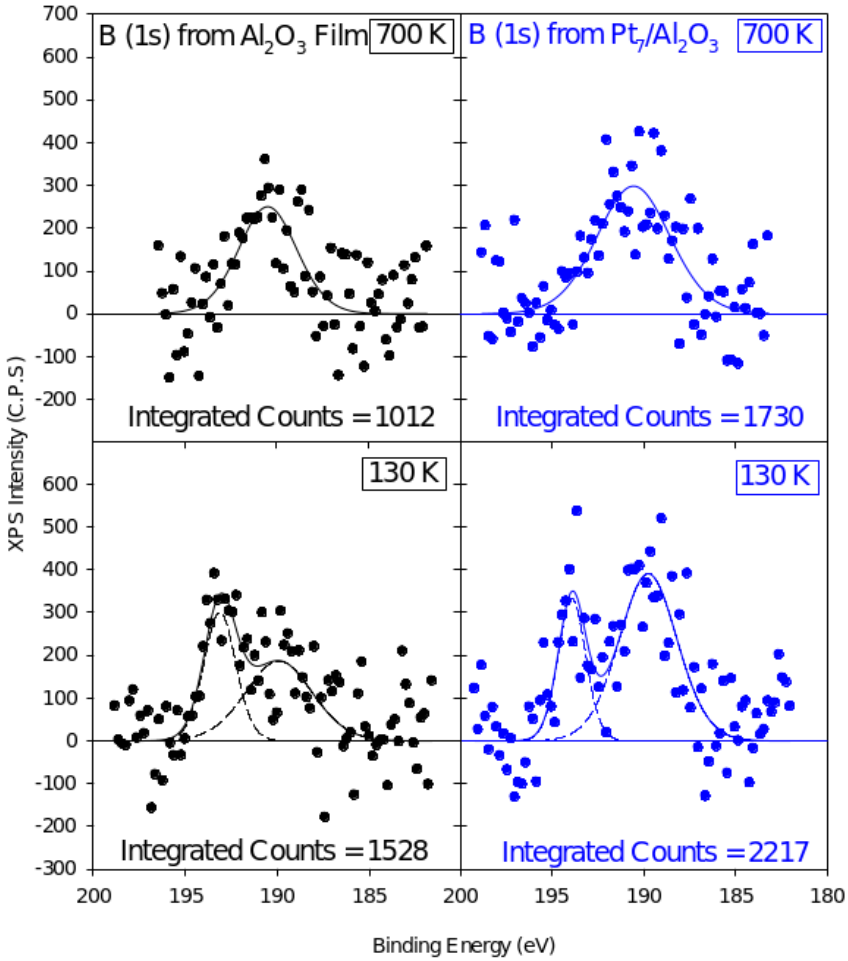

Figure 2. XPS spectra obtained for both Pt-free alumina (black) and Pt_7/alumina (blue) samples following exposure to 3 L of B_2H_6 at 130 K and after heating to 700

which showed ~13% less desorption of boron-containing species when Pt_7 was present (at 10% coverage). Taken together, both TPD/R and XPS show that substantially more boron adsorbs when Pt_7 is present, but that less desorbs, i.e., the presence of a low coverage of Pt_7 leads to substantially more boron deposition on the samples.

C. Temperature-dependent ion scattering spectroscopy: The final experimental probe of diborane-surface interactions was temperature-dependent He^+ ion scattering (TD-ISS). TD-ISS involves cooling the sample, exposing it to an adsorbate of interest, then monitoring changes in ISS intensities as the sample is heated. A typical raw ISS scan (Figure S4) shows distinct peaks for single scattering from Pt, O, and Al atoms in the surface layer,[35] along with a featureless background due to multiple and subsurface scattering. As discussed previously,[12, 14] Pt_7 deposits in an ensemble of prismatic and single layer structures, with most of the Pt in the surface layer, and thus detectable by ISS. Adsorbates attenuate ISS signals from the underlying surface through a combination of shadowing, blocking, and reduced ion survival probability.[35, 40] For our scattering geometry, attenuation primarily affects signal from atoms directly under, or surrounding, the adsorbate. Thus, adsorbates binding directly on top of the Pt clusters attenuate Pt signal, with little or no effect on Al or O signals. Conversely, adsorption on the alumina film, or at sites around the periphery of the clusters, tends to attenuate Al and O signals, with little or no effect on the Pt signal. As heating drives desorption, the attenuated ISS signals should tend to recover toward the adsorbate-free values. To the extent that diborane exposure and heating leads to cluster agglomeration, forming larger multilayer Pt particles, this would reduce the fraction of Pt in the surface layer, and thus the Pt ISS signal.

As shown in Figure S4, there is no obvious ISS signal for boron ($E/E_0 \approx 0.26$) in the spectrum taken immediately after diborane exposure at 110 K, nor is B ISS signal observed after heating the sample, despite the evidence that boron must be present on these samples (Figures 1 and 2). Lack of boron signal could be taken as evidence that boron is not in the surface layer, however, boron may simply have been undetectable due to a combination of low coverage, small He^+-B scattering cross section ($\propto$ target atomic number^{35}), and high multiple-scattering background at low E/E_0.

Figure 3 compares the Pt, O, and Al ISS signals as a function of temperature, for a Pt_7/alumina sample that was exposed to 1.5 L of B_2H_6 at 110 K, probed by ISS, and then heated to 700 K in 50 K steps, with an ISS measurement made at each temperature. All spectra were collected with low (0.1 μA) He^+ flux impinging at 45° and detected along the surface normal, with 30 second scan time used to minimize sample damage. The horizontal dashed lines show the Pt, O, and Al intensities

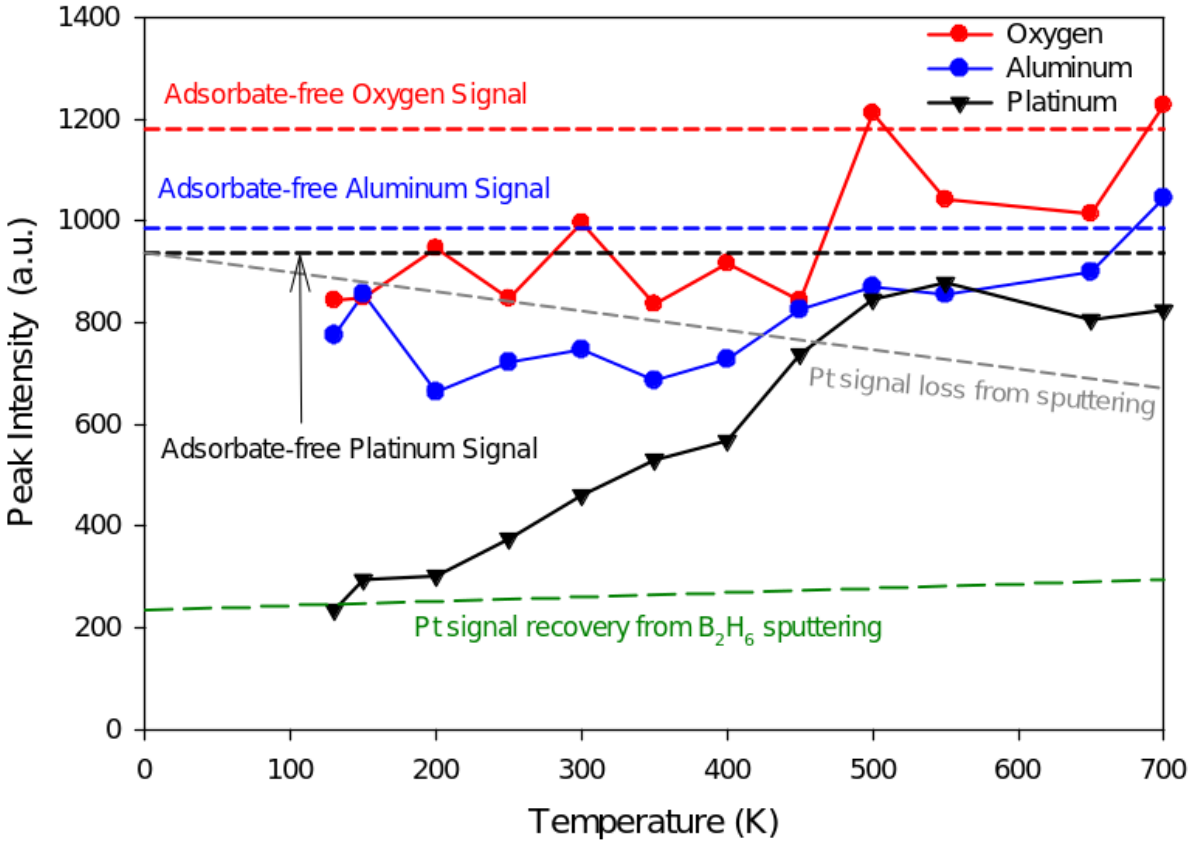

Figure 3. TD-ISS of Pt_7/alumina exposed to 1.5 K of diborane at 110 K. The intensities for adsorbate-free Pt_7/alumina, measured separately, are indicated as horizontal dashed lines. The effects of He^+ sputtering on Pt signal in adsorbate-free and diborane-dosed Pt_7/alumina held at 110 K are shown as dashed lines labeled "Pt signal loss from sputtering" and "Pt signal recovery from B_2H_6

measured for adsorbate-free Pt_7/alumina in a separate experiment. Compared to these adsorbate-free values, the signals measured after the B_2H_6 dose are attenuated by ~80% for Pt and ~20% for O and Al, indicating that B_2H_6 binds preferentially in sites that attenuate Pt ISS signal. ISS, thus, is consistent with the XPS and TPD/R results indicating that diborane binds preferentially in association with Pt_7, and provides the additional insight that some or all of this Pt-associated diborane binds on top of the clusters, where it attenuates scattering from underlying Pt. The ~20% attenuation of Al and O signals indicates that some diborane binds in sites that shadow or block scattering from alumina, which could include both sites around the periphery of the clusters, and on the alumina film remote from the clusters.

Interpretation of changes in signal as the sample is heated requires knowledge of the effects of He^+ bombardment occurring during the repeated ISS scans used in TD-ISS. To probe the rate of Pt loss by sputtering, an experiment was made on a separate adsorbate-free Pt_7/alumina sample, held at constant temperature, while taking a series of ISS spectra. The rate of Pt ISS signal decrease is indicated in Figure 3 by the dashed line labeled “Pt signal loss from sputtering”. Conversely, for a diborane-covered Pt_7/alumina sample held at 110 K, the Pt signal slowly increased during successive ISS scans, due to sputtering of adsorbates initially bound on top of the clusters, as indicated by the line labeled “Pt signal recovery from B_2H_6 sputtering”. The Al and O ISS signals were not observed to change significantly in either control experiment, presumably because the diborane coverage on alumina is low, and sputtering of Al or O from the top layer simply exposes more Al and O in the 2^{nd} layer.

As shown in Figure 3, the Pt ISS signal starts to recover significantly faster than

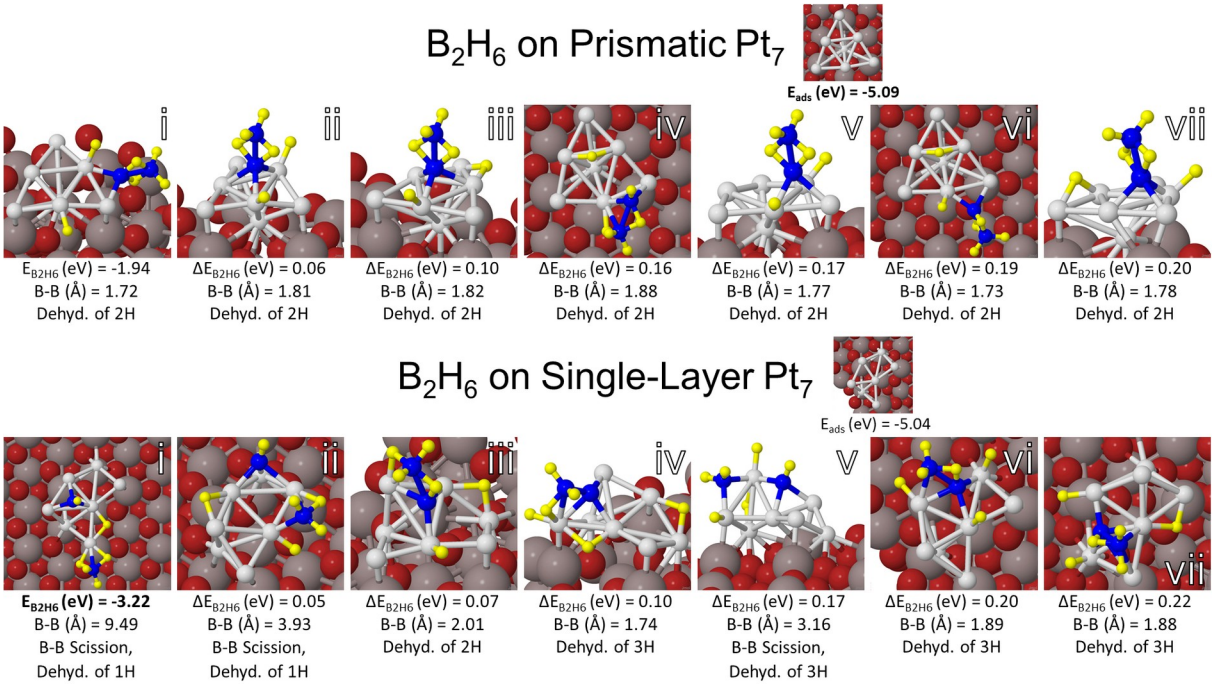

Figure 4. The seven lowest minima of diborane (B_2H_6) adsorbed on the two lowest minima of Pt_7, which also represent two different structural classes of Pt clusters, i.e., "prismatic" and "single-layer". The most stable adsorbate-free Pt_7/alumina isomer is prismatic, but with diborane adsorbed the single layer isomer becomes more stable by over 1 eV. Boron atoms are depicted in blue, platinum in light gray, hydrogen in yellow, aluminum in dark gray, oxygen in red.

would be expected from B_2H_6 sputtering at ~200 K, gradually recovering to ~95% of the adsorbate-free value by ~550 K, then is constant at higher temperatures. The Al and O signals remain attenuated up to ~450 K but then recover to their adsorbate-free values by 700 K.

D. DFT results for adsorption of diborane on Pt_7 clusters: PW-DFT calculations were performed to identify low energy adsorption geometries for diborane on Pt_7/alumina, as summarized in Figure 4. We previously reported on the energetics and geometries of numerous isomers of Pt_7 and Pt_8 bound to alumina.[14] Here, we focus on adsorption of diborane on the two lowest energy minima of

Pt_7/alumina, which are shown in the small figures next to the titles of each section of Figure 4. The most stable Pt_7/alumina structure is prismatic (E_{ads} = -5.09 eV, relative to alumina + gas phase Pt_7), but there is a single-layer isomer that is only slightly higher in energy (E_{ads} = -5.04 eV). Seven different isomers of diborane adsorbed on both prismatic and single layer Pt_7/alumina are shown, all of which would contribute to the population at 700 K and below, according to Boltzmann statistics. In these 0 K, *in vacuo* calculations, the most stable configurations of diborane on the prismatic Pt_7 cluster preserve the B-B bond and are adsorbed atop or peripherally to the cluster. On single-layer Pt_7, however, the most stable structures involve B-B bond scission.

There are several factors to bear in mind in comparing theory to experiment. Due to computational limits, our DFT calculations were restricted to adsorption of only a single diborane and focused on the strongest diborane binding sites, i.e., diborane binding on the clusters. The experimental diborane coverages were higher and populated binding sites on both Pt_7 and the alumina film. As a result, the calculations cannot address complex chemistry such as higher borane formation and desorption. In addition, while the minima found by DFT clearly illustrate a variety of binding arrangements, we cannot guarantee that they represent all possible low energy binding geometries. Indeed, the fluxionality of these clusters is important in their catalysis but also resists facile theoretical description.[6, 14, 41-44] The complexity of the problem will certainly increase at elevated temperatures or for increasing coverage of B_2H_6.

For prismatic Pt_7/alumina, the most stable isomer in absence of adsorbates, diborane adsorbs atop or at peripheral sites on the cluster. The B-B bond is preserved with only one or two H atoms transferred from diborane to Pt sites. The

B-B bond lengths range from 1.72 to 1.88 Å, compared to 1.76 Å calculated for gas-phase diborane (Figure S6), in excellent agreement with the experimental value (1.7645 Å).[45] Relative to prismatic Pt_7/alumina + gas phase B_2H_6, the most stable binding geometry for diborane on prismatic Pt_7 has E_{ads} = -1.94 eV, and the other structures shown are all within 0.2 eV (ΔE_{ads}). The atomic charges for the various isomers of diborane adsorbed on prismatic Pt_7/alumina are shown in Figure S7.

Diborane binds more strongly to the single layer Pt_7/alumina isomer, with E_{ads} = -3.22 eV for the most stable structure. Note that three of the seven isomers shown involve B-B bond scission and other isomers feature a B-B bond elongated by 7-14% compared to gas-phase B_2H_6. All isomers involve transfer of up to three H atoms from B to Pt sites. The atomic charges for the various isomers of diborane adsorbed on single layer Pt_7/alumina are shown in Figure S8.

The substantially higher E_{ads} for diborane on the single layer Pt_7 isomer implies that with one diborane adsorbed, single layer Pt_7/alumina becomes the global minimum by ~1.2 eV. The barrier height for diborane-induced isomerization from the prismatic local minimum to the single layer global minimum is unknown, but comparison with ethylene adsorption is suggestive. DFT also found that ethylene adsorbed more strongly on single layer Pt_7/alumina (E_{ads} = -1.97 eV), compared to prismatic Pt_7/alumina (E_{ads} = -1.29 eV), and in that case, adsorption of three ethylene molecules was sufficient to eliminate the prismatic-to-single-layer isomerization barrier for Pt_7.[14] The difference in adsorption energy for diborane on the two Pt_7 isomers is almost twice as large as the difference for ethylene, suggesting that isomerization is not unlikely at the diborane exposures used in the experiments.

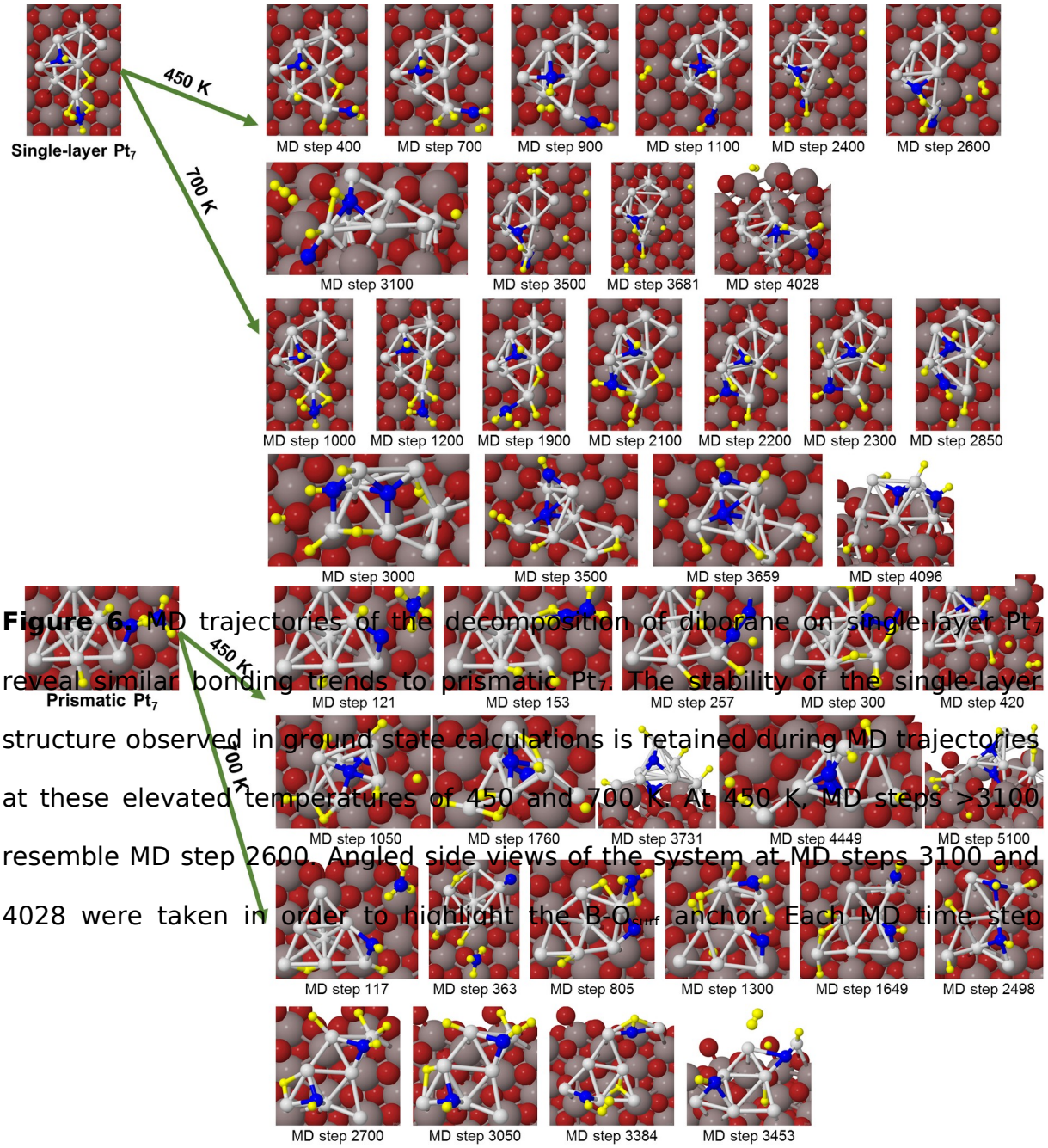

Figure 6. MD trajectories of the decomposition of diborane on single-layer Pt_7 reveal similar bonding trends to prismatic Pt_7. The stability of the single-layer structure observed in ground state calculations is retained during MD trajectories at these elevated temperatures of 450 and 700 K. At 450 K, MD steps >3100 resemble MD step 2600. Angled side views of the system at MD steps 3100 and 4028 were taken in order to highlight the B-O_{surf} anchor. Each MD time step

Figure 5. MD trajectories of diborane decomposition on prismatic Pt_7 reveal that diborane may either split apart to form a B-O_{surf} anchor or maximize Pt-B bonds by adsorbing onto a Pt cluster facet. The prismatic structure can also distort significantly or form a flattened, single-layer geometry. At 450 K, beyond 3.0 ps, the cluster changed very little with only the hydrogens translating from one atom

E. Molecular dynamics simulations of diborane/Pt_7/alumina thermal chemistry: To probe adsorbate effects and chemistry at the elevated temperatures used in the experiments, we used Born-Oppenheimer MD simulations to examine the fate of diborane adsorbed on Pt_7 at 450 and 700 K. Both of these temperatures are well above the range where B_nH_m desorption is observed (Figure 1) and in the range where H_2 desorption occurs on Pt clusters (Figure S5). This is also the range of interest for ethylene dehydrogenation, which peaks near 450 K for Pt_7/alumina and goes to completion below 700 K.[14] The prismatic and single-layer minima of Pt_7 represent different initial geometries for diborane to adsorb and react on. Selected highlights from MD trajectories on each structure at both temperatures are given in Figures 5 and 6, respectively (each MD time step corresponds to 1 fs).

Starting with the lowest energy minimum for diborane on prismatic Pt_7, MD shows that at these elevated temperatures diborane undergoes B-B scission to form BH_2, BH_3, or BH_4 fragments, which may then re-adsorb onto Pt sites (Figure 5). Interestingly, in the 450 K trajectory, diborane dehydrogenated completely with one of the boron atoms moving to a position underneath the Pt_7 cluster, forming Pt-B-O_{surf} bonds and anchoring the cluster to the alumina surface. In contrast, in the 700 K trajectory, the Pt cluster flattened to a triangular, single-layer structure with BH fragments maximizing the number of Pt-B bonds. Throughout the MD trajectories, at both temperatures, hydrogen atoms are mobile, translating to adsorb onto the Pt cluster, to Al, O atoms on alumina, or forming H_2 (shown desorbing from the surface). Moreover, both the 450 and 700 K MD trajectories favored B-B bond scission early on, within the first 120 fs of the simulation.

Starting with lowest energy isomer of diborane on single-layer Pt_7, at either 450 or 700 K, the Pt cluster retains much of its structure with B or BH_y fragments making

small translations (Figure 6). Similar to the prismatic Pt cluster, at 450 K, diborane's boron atoms either sit on top of the cluster to maximize Pt-B bonds or move below the cluster to form Pt-B-O_{surf} anchor bonds. At 700 K, BH fragments sit on the Pt cluster facets, forming 3-4 Pt-B bonds.

Due to computational time limitations, we were only able to run a few trajectories, following the dynamics for ~5 ps. Of course, the MD picture is incomplete, and only accesses a small portion of configurational space accessible to our systems. Nonetheless, these MD results give insight into possible decomposition mechanisms of diborane on alumina-supported Pt clusters. One obvious point is that Pt, B, and H atoms are all mobile at these temperatures, consistent with the DFT finding of numerous structures within a few tenths of an eV of the global minimum. By the end of the trajectories, the Pt_7 clusters remained intact, but most of the initial B-H bonds had broken, with H atoms binding instead to Pt or to O atoms of the support, and some H atoms recombined to form H_2 seen desorbing from the surface, even on the relatively short time scale of the trajectory. Boron atoms prefer to bind either under the cluster, forming Pt-B-O_{surf} linkages, or to facets of the Pt clusters, forming multiple Pt-B bonds. Boron atoms bound to Pt facets may block preferred carbon adsorption sites or weaken carbon adsorption, which may account for the observed resistance to coking of borated Pt clusters.[4-6] However, B bound between the cluster and the support also affects the affinity to C by altering the electronic structure of the system, particularly, the charge transfer from the support to the cluster, as was shown previously.[6]

At the higher diborane coverages of the experiments, additional processes, presumably, would occur, such as coupling of BH fragments to form higher boranes that might desorb (Figure 1) and more extensive recombinative desorption of H_2.

Over longer time scales, particularly at 700 K, additional hydrogen desorption would almost certainly occur, leaving behind Pt_7B_x clusters. The simulations suggest that the Pt_7B_x clusters would have a range of Pt morphologies (prismatic and single-layer) and boron binding sites (Pt facets, Pt-B-O_{surf}), and the cluster structures are likely fluxional at high temperatures.

F. Pt_4B_4/alumina: As a computationally tractable model for Pt_nB_m clusters with higher boron mole fraction, as probably form in the experiments, we chose to study Pt_4B_4 clusters. The global optimization search for gas-phase and adsorbed Pt_4B_4 was performed utilizing the Basin Hopping method,[24] and the set of low energy isomers is shown in Figures 7 and S9 for Pt_4B_4/alumina and gas-phase Pt_4B_4, respectively. Both gas-phase and adsorbed Pt_4B_4 structures tend to be (quasi-)planar. Huynh, et. al. ascribed the drive towards planarity with increasing boron concent ration to the covalent nature of boron-boron bonds and boron-metal bonding in mixed metal-boron clusters in B_nAl_{6-n} and LiB_nAl_{6-n} systems, and proposed that this effect may be general to other metal-boron systems.[4-6, 46] Noticeably, their study found the transition from predominantly 3D to 2D structures occurs when the Al:B ratio is 1:1. The Pt-B clusters seem to follow a similar pattern, with the single-layer geometry dominating in gas-phase Pt_4B_4 (isomers i-iii, see SI) as compared to Pt_7B (isomers v).[6]

For alumina-supported Pt_4B_4, the Pt_4 moiety is also near-planar, however, the B atoms tend to be bent toward the alumina support to allow formation of short B-O_{surf} bonds anchoring the Pt_4 moiety to the alumina. The B-B bonds in surface-bound clusters are ~1.7 Å, and Pt-B bonds are ~2 Å. The results also show that, even for high boron concentrations, the energetically favorable structures have all the Pt atoms in the surface layer, with most or all of the B atoms underneath the clusters.

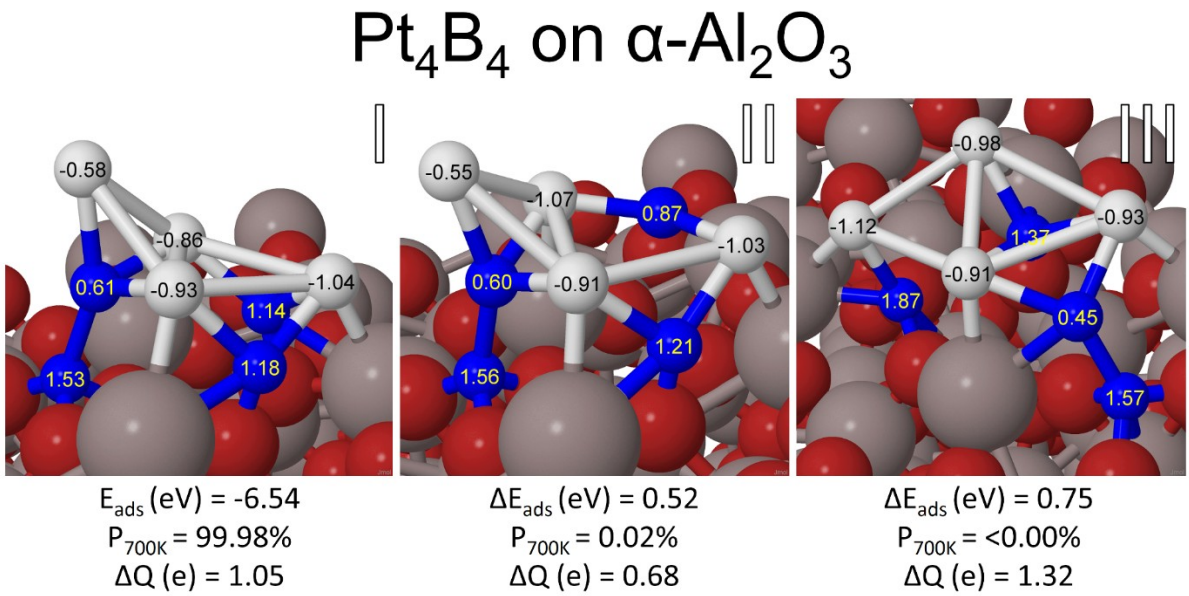

Figure 7. The three lowest minima of Pt_4B_4 adsorbed on alumina with their associated adsorption energies (E_{ads}), Boltzmann populations at 700 K (P_{700K}), and Bader charges on individual atoms. Boron atoms are depicted in blue, platinum in light gray, aluminum in dark gray, oxygen in red. Isomer II is very similar to Isomer I but with a B-O_{surf} anchor broken.

This has important implications for interpretation of the TD-ISS results, and also means that all the Pt atoms are exposed and available to act as catalytic sites.

In previous publications, we predicted that addition of electropositive boron would temper the highly active and electronegative Pt clusters by reducing the charge of the cluster.[6, 47] High electron density favors ethylene adsorption in sp^3-hybridized geometries, a precursor to dehydrogenation. On the other hand, sp^2-hybridization tends to favor hydrogenation or desorption.[1, 3, 48-50] In pure Pt_7 and Pt_8 clusters on alumina, Pt atoms were found to have charges ranging from +0.78 e, when bound primarily to O_{surf}, to -0.73 e, when bound primarily to Al_{surf}, with net cluster charge being ca. -1 e.[14] For Pt_7B on alumina, the net charge on the clusters dropped to ca. -0.35 e, with strong variations from one isomer to another.[6] With

increasing boron content, Pt_4B_4 clusters on alumina become positively charged, between +0.68 and +1.32 e. In addition, the charge separation between Pt and B atoms increases with increasing boron concentration: Pt remains negative, ranging from -0.5 to -1.1 e, and B atoms are positively charged, between +0.4 e, when forming a mix of Pt-B or B-B bonds within the cluster, and +1.87 e, when forming a $B\text{-}O_{surf}$ anchor. Increasing the B:Pt ratio also increases the stability of supported Pt-B clusters with Pt_4B_4 adsorbing more strongly by ~1.9 eV as compared to Pt_7B (E_{ads} = -4.62 eV[6]). This may be attributed to the cluster maximizing $B\text{-}O_{surf}$ interactions and optimizing the electrostatic attraction between the electronegative Pt atoms and electropositive B atoms with a 1:1 ratio of Pt:B.[51]

IV. Discussion

From our previous study of ethylene dehydrogenation on borated Pt clusters, we know that boration of Pt_7/alumina substantially reduces the ethylene desorption temperature, resulting in a significant decrease in the fraction of ethylene that undergoes unwanted dehydrogenation.[6] The obvious questions are how much boron is deposited on the Pt_7/alumina surface by the boration process used, and in what kinds of binding sites is it found.

Figure 1 shows that quite complex chemistry occurs when diborane is adsorbed on both alumina and Pt_7/alumina surfaces. The chemistry is qualitatively similar for the two surfaces, reflecting the fact that the Pt_7 coverage is only 10%. Similarities include the low intensity for diborane desorption (mass 26), and higher intensities for desorption of both BH_x (mass 11) and higher boranes such as tetraborane (mass 48) and pentaborane (mass 59). The fact that desorption is dominated by B_1 or B_n ($n \geq 4$) species indicates that adsorbed diborane dissociates at low temperatures, undergoing complex recombination chemistry.

The DFT results support this conclusion, showing that, even at 0 K, diborane spontaneously loses H atoms on both prismatic and single layer Pt_7, and that on the single layer isomer, B-B bond scission also occurs. Given that the single layer isomer becomes the global minimum upon diborane adsorption, extensive diborane decomposition is expected. That expectation is supported by the MD trajectory results, in which B-B bond scission and Pt_7 isomerization is observed on the picosecond time scale at moderate temperatures. Experimentally (Figure S5) and computationally (Figure 6), hydrogen recombinative desorption is observed at moderate temperatures, suggesting that the final state of the borated Pt_7/alumina samples consists primarily of Pt and B atoms, binding in some fashion to the

alumina support.

The XPS results in Figure 2 show that a significant fraction of the boron initially adsorbed as diborane is left behind after thermal desorption is complete. The amount of boron on the surface can be estimated from XPS peak intensities. For this analysis we take advantage of the fact both Pt and B are deposited on the sample surface at low coverage, and that we know the amount of Pt deposited quite precisely (1.5×10^{14} Pt atoms/cm^2). Attenuation by inelastic scattering can be neglected for photoelectrons emitted by atoms in the surface layer, thus for the Pt_7/alumina sample, the B/Pt coverage ratio can be calculated from the ratio of integrated B 1s and Pt 4d intensities. The only information needed for this calculation is the ratio of B 1s and Pt 4d photoemission cross sections, for which we used theoretical cross sections reported by Yeh *et al.*[34] ($\sigma_{B1s} = 6.6 \times 10^{-3}$ Mb, $\sigma_{Pt4d} = 2.64 \times 10^{-1}$ Mb), which we checked against empirical atomic sensitivity factors[52] taking the electron attenuation length into account.[53] (For our 54.7° x-ray source-analyzer angle, photoemission asymmetry can be neglected).[54] For the Pt-free alumina sample, we determined the boron coverage by comparison to the Pt_7/alumina sample studied under identical conditions. Because of the extremely weak B 1s signal (Figure 2), the resulting boron coverages are estimated to have uncertainties of ±40%.

For the Pt-free alumina film, this analysis gives a boron coverage immediately after 130 K diborane exposure of ~9.8 B atoms/nm^2 corresponding to ~5 B_2H_6/nm^2. From its structure, we can estimate that an intact diborane molecule lying flat on a surface would occupy roughly 0.06 nm^2, thus the boron coverage is equivalent to roughly 30% of a close-packed monolayer. That can be compared to the ~20% attenuation of Al and O ISS signals observed after 130 K diborane exposure in the

ISS experiment (Figure 3). After heating the alumina sample to 700 K, the B 1s signal decreased by ~34% to ~6.5 B/nm^2, compared to ~15 O atoms, and 10 Al atoms *per* nm^2 of the alumina film.

For the sample containing 0.2 ML-equivalent of Pt_7 clusters, the amount of B_2H_6 adsorbed at 130 K increased to ~14.2 B/nm^2 or ~7 B_2H_6/nm^2. If we assume the diborane coverage on the alumina portion of the 0.2 ML Pt_7/alumina sample is just 0.8 of the coverage observed on Pt-free alumina, we can estimate that ~4 of the B_2H_6 molecules are on alumina sites, and ~3 are associated with Pt sites. This 0.2 ML-equivalent sample had 0.43 Pt_7 clusters deposited *per* nm^2, leading to the conclusion that ~7 diborane molecules are associated with each Pt_7 cluster. The large attenuation of Pt ISS signal upon diborane exposure (Figure 3) shows that a significant fraction of the Pt-associated diborane is bound in sites on top of the clusters, but we cannot rule out some diborane in sites around the cluster periphery. We note that for a single B_2H_6, DFT found that diborane fragments occupy both “on top” and peripheral sites (Figure 3). Heating the sample to 700 K resulted in final B coverage of ~11 B/nm^2. On Pt-free alumina, the final B coverage was 6.5 B/nm^2, thus from the 80:20 alumina:Pt area ratio, we can estimate that of the 11 B/nm^2, ~5.2 are bound to alumina sites, and the remaining ~5.8 B are bound to Pt sites, or 13.5 B atoms/Pt_7. Prior to heating, there were 7 diborane molecules = 14 B atoms in Pt-associated sites. This observation suggests that diborane initially adsorbed in Pt-associated sites decomposes during heating, leaving nearly all of its boron atoms on the surface. The implication is that essentially all the boranes desorbing from Pt_7/alumina (Figure 1) can be attributed to diborane initially adsorbed on alumina sites. If that conclusion is correct, we would expect ~10% less

borane desorption from 0.1 ML Pt_7/alumina, compared to Pt-free alumina, which is reasonably consistent with the observation of ~13% less desorption.

The B 1s binding energies also provide insight into the nature of the binding. Diborane adsorbed at 130 K on Pt_7/alumina gives rise to a high binding energy peak at 193.9 eV and a broader low binding energy feature that peaks around 189.7 eV. For diborane on alumina, there is a peak at 193.1 eV with similar intensity to that for Pt_7/alumina but the signal at low binding energies is much weaker than for the Pt_7/alumina. The higher binding energy features are in the energy range (193 – 193.7 eV) typically reported for fully oxidized boron (B^{3+}) in compounds such as boron oxide or boric acid.[55] Elemental boron (B^0) is reported to have binding energies around 188 eV,[55] thus the broad 189.7 eV features are suggestive of boron in some partially oxidized form, which obviously is more prevalent when Pt_7 is present. DFT was used to calculate the charges for a single diborane on both prismatic and single layer isomers of Pt_7/alumina, as shown in Figures S7 and S8, respectively. It can be seen that roughly half the boron atoms in the various isomers tend to be fully oxidized (B^{3+}), and half are in intermediate oxidation states ($B^{1.5+}$ to $B^{1.6+}$). These results appear to be in good agreement with the observed binding energies. It should be noted, however, that for the higher diborane coverages in the experiments, higher boranes form on the surface. B 1s binding energies for such species are not known, but we note that an orthocarborane ($B_{10}C_2H_{12}$) film deposited on copper is reported to have B 1s binding energy of 189.3 eV,[56] also in reasonable agreement with the lower binding energy feature. For reference, in previous studies of low temperature diborane adsorption/decomposition on Mo(100) and Ni(100) two B 1s peaks were observed at 189.2 eV and 187.6 eV, but in those experiments the boranes were binding directly

to metals, rather than oxides.

After heating to 700 K, both alumina and Pt_7/alumina samples show a single broad B 1s peak at ~190.5 eV, suggesting boron is present in a distribution of intermediate oxidation states. This conclusion is broadly consistent with the distribution of boron oxidation states ($B^{0.5+}$ - $B^{1.9+}$) found for B atoms in Pt-B-O_{surf} bridge bonds, as shown for Pt_4B_4 in Figure 7.

In summary, XPS indicates that at 130 K, diborane adsorbs preferentially in association with Pt clusters, compared to the alumina support, and that little, if any, of this Pt-associated boron desorbs during heating to 700 K. As a result, the boration process investigated leaves Pt clusters with much larger boron coverages than the alumina support. The final B:Pt ratio for the clusters is estimated to be quite high, but we note that the absolute coverages are uncertain by ~ ±40%, due to the very weak B 1s signal. Note also that both the cluster coverage and diborane exposure used in these XPS experiments was twice those for all the other experiments. It is not clear how these changes might have affected the amount of boron deposited *per* cluster, however, we did study how the diborane exposure used in boration affected subsequent ethylene TPD/R. Boration with 0.5 L diborane exposure was found to be almost as effective at suppressing dehydrogenation as boration with 1.5 L exposure, i.e., at least the *chemical effects* of boration appear to saturate at exposures below those used in all the experiments described in this report.

XPS also shows that the boration process leads to some boron deposition on the alumina film support, thus it is important to know how the catalytic properties of the samples are affected by the boron atoms on (or in) the support. To address this

question, Figure 8 compares the ethylene adsorption, desorption and dehydrogenation behavior of three samples:

1. As-deposited Pt_7/alumina with no boron exposure ("Pt_7/alumina"). 2. Pt_7/alumina borated after cluster deposition, i.e. both Pt_7 and alumina with boron ("B/Pt_7/alumina"). 3. Pt_7 deposited on a pre-borated alumina support, i.e., only the

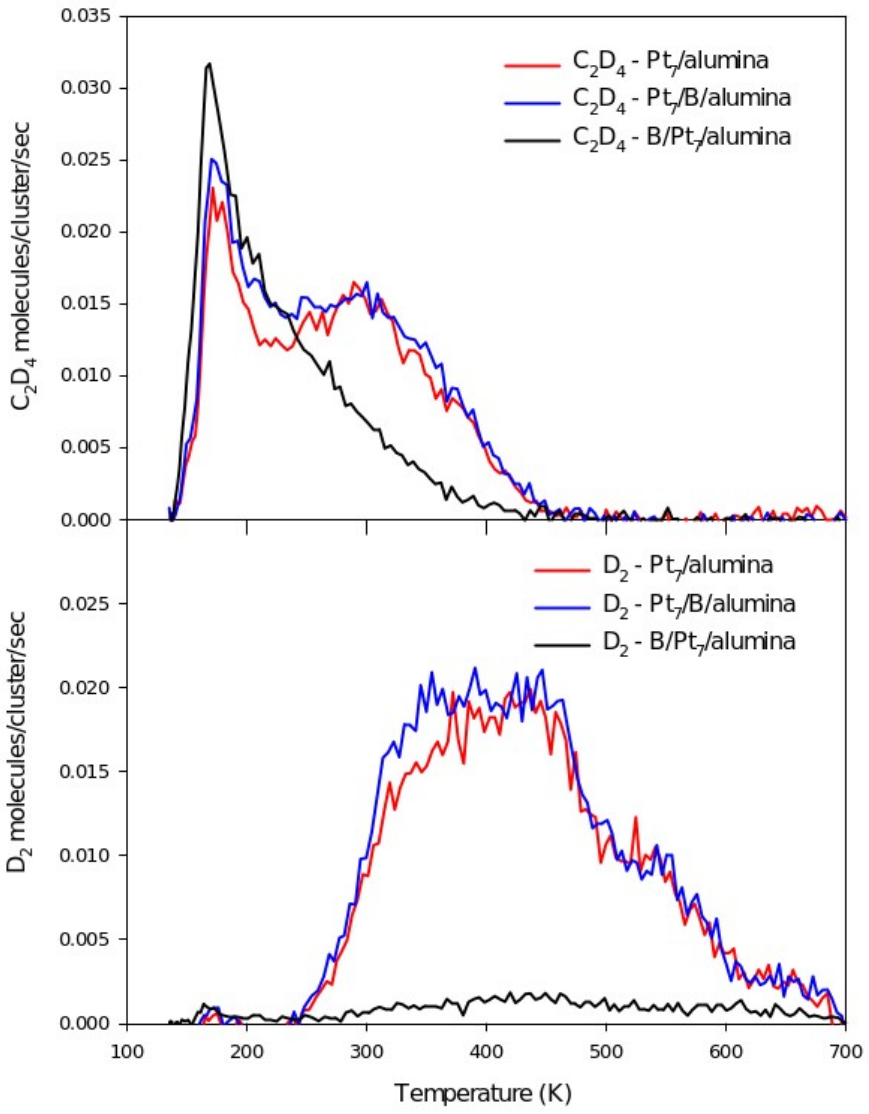

Figure 8. Thermal desorption spectra of unreacted ethylene and deuterium product obtained from three samples: (Red) As-deposited Pt_7/alumina with no boron exposure, (blue) Pt_7 deposited on pre-borated alumina, and (black) Pt_7/alumina borated after Pt_7 deposition. Each sample was exposed to 5 L C_2D_4 at 150K. Boration was done using our standard method (1.5 L B_2H_6 at 130 K, heating

alumina was borated ("Pt_7/B/alumina"). Boration was done using our standard method (1.5 L B_2H_6 exposure at 130 K, followed by heating to 700 K), and ethylene TPD/R was carried out under conditions identical to those used in our previous studies[6, 14] (5 L C_2D_4 exposure at 150 K, heating at 3 K/sec to 700 K). Ethylene desorbs from Pt_7/alumina in two components. The low temperature feature was shown to result from ethylene desorbing from defect sites in the alumina film, and the broad feature peaking near 300 K results from ethylene adsorbed at Pt_7 sites.[14] A substantial amount of D_2 desorption is observed above 300 K for Pt_7/alumina, but none is observed for the alumina film alone.

Boration of both the clusters and the support (B/Pt_7/alumina) leads to a substantial decrease in the desorption temperature distribution for ethylene, and near-total attenuation of D_2 desorption. In contrast, borating only the alumina support (Pt_7/B/alumina) has little effect on the Pt_7 chemistry. The low temperature ethylene desorption feature attributed to desorption from the alumina support is less intense and sharper for this sample, suggesting that boration of the alumina support weakens the ethylene-alumina binding, possibly due to boron occupying alumina defect sites. Pre-boration has little effect, however, on the amount or temperature dependence of ethylene desorbing from Pt sites, or on the D_2 production, suggesting that the presence of a small amount of boron in the support has little effect on supported Pt clusters. Clearly, the large effects of boron on chemistry of supported Pt clusters are due to boration of the Pt clusters, rather than the support.

XPS probes boron on the surface, thus providing an indirect method to estimate the fraction that desorbs during heating. TPD/R (Figure 1) provides a complementary probe of the desorbing fraction, provided that we can convert the

measured $B_xH_y^+$ ion signals to fluxes of various neutrals desorbing from the surface. It is impractical to directly calibrate the mass spectrometer for detection of species such as BH_3, tetraborane, or pentaborane (toxic, pyrophoric, not commercially available), but we can do an approximate analysis. We previously calibrated the ion intensity – neutral desorption relationship for C_2D_4,[14] which should have EI cross section similar to that for B_2H_6, and also has similar EI cracking behavior. For desorbing BH_x, B_4H_{10}, and B_5H_9, we note that the EI cross section should scale roughly with number of B atoms, i.e., the total ionization signal should increase roughly linearly with borane size. The extent of EI cracking also increases with borane size,[37] however, such that the fraction of the ion signal appearing at the detected mass values decreases with size[6]. As a result of these two factors, we expect that the detection sensitivity for the various borane products should be similar, and that they should be similar to that for ethylene. Using this crude approximation, we can estimate that of the ~5 B_2H_6 molecules found by XPS to be adsorbed at 130 K, the equivalent of ~0.9 B_2H_6/nm^2 (~20%) desorbs in the form of various boranes, which is in reasonable agreement with the ~30% desorption estimated from XPS. For Pt_7/alumina, ~7 B_2H_6/nm^2 adsorb at 130 K, but only the equivalent of ~0.80 B_2H_6/nm^2 (~11%) desorb, compared to ~21% boron desorption estimated by XPS. Considering the crude approximations required for this analysis, and low XPS signal, the TPD and XPS results are in reasonable agreement regarding the amount of boron lost during heating.

Figures S2 and S3 give the desorption energy distributions for the various borane products observed, all of which are below 0.5 eV. The DFT adsorption energies for diborane on Pt_7/alumina are all much higher – ranging up to ~3 eV on the single layer isomer. This discrepancy is easily explained. The DFT calculations

were done to find the structure and energetics for a single diborane molecule in the strongest binding sites, which are on the Pt clusters. The experiments were done at much higher diborane coverages and include diborane bound to Pt sites and to the alumina film. As shown by XPS, boron bound to the Pt clusters does not desorb during heating, thus the TPD/R experiments are only sensitive to boranes desorbing by recombination of B_xH_y and H adsorbed on the alumina support, where the binding energies are clearly much lower than for Pt-associated sites.

XPS shows the amount of boron associated with Pt, but provides no insight into the nature of the boron-Pt binding. TPD/R gives the temperature ranges in which boranes (Figure 1) and hydrogen (Figure S5) desorb, but provides no insight into the sites they desorb from. Analysis of the TD-ISS results (Figure 3) in light of the XPS and TPD data provides some of this structural information. The large attenuation of Pt ISS signal, and much smaller attenuations of Al and O signals, are consistent with the XPS results. Both show that diborane adsorbs more efficiently in association with the Pt clusters than on alumina sites, and ISS shows that a significant fraction adsorbs on top of the clusters where it attenuates Pt signal. Figure 1 shows that desorption of B_nH_m species is complete by ~200 K, thus it is surprising that there is no significant recovery of Pt, O, or Al ISS signals as the sample is heated to 200 K. Recovery of the Pt ISS signal occurs in two stages at higher temperatures. Between 200 and 400 K, the Pt signal increases to about half the expected value for adsorbate-free Pt_7. This is the temperature range in which hydrogen desorbs from Pt_7 (Figure S5), suggesting that desorption of hydrogen exposed some Pt atoms but that ~half the Pt atoms remained blocked by adsorbed boron. This conclusion is consistent with the XPS results indicating that little of the

boron associated with Pt sites desorbs, i.e., the borane desorption observed in TPD/R originates almost entirely from the alumina film.

Between 400 and 550 K, the Pt signal recovers to almost the adsorbate-free limit. Since nothing desorbs in this temperature range, the recovery of Pt ISS signal must reflect a structural change in the Pt clusters, and the DFT results suggest the explanation. Both the MD simulations (Figures 5 and 6) and the structures found for adsorbed Pt_4B_4 indicate that the most stable binding sites for boron atoms in Pt_nB_m clusters are in Pt-B-O_{surf} bridging sites, where the B atoms are under the Pt cluster, anchoring it to the surface. As a result, the Pt atoms are in surface layer and detectable by ISS.

The fact that the Pt ISS signal recovers to 95% of the value for adsorbate-free Pt_7 also suggests that sintering or agglomeration of the clusters during the boration process is limited, because either process would tend to form larger, 3D clusters in which a smaller fraction of Pt is in the ISS accessible surface layer. Indeed, the final Pt ISS signal is well above what would be expected from He^+ sputtering of Pt during the series of ISS scans. This, too, is consistent with the XPS results, which indicate high diborane coverage on the Pt clusters, which would tend to shield the underlying Pt from most of the sputtering that occurs for adsorbate-free clusters.

V. Conclusions

We have shown that diborane exposure followed by heating, preferentially deposits boron atoms on supported Pt clusters, with a much smaller boron coverage on the alumina support. The boron on the alumina support is shown to have essentially no effect on ethylene binding or dehydrogenation on the supported Pt clusters. Therefore, the weakening of the ethylene binding and suppression of dehydrogenation when Pt_n/alumina is borated can be attributed to boron atoms

associated with the Pt clusters. This boron is found by DFT, in agreement with TD-ISS, to move to sites beneath the Pt clusters, forming Pt-B-O_{surf} bonds that anchor the clusters to the support.

Associated Content

Supporting Information: Supplemental experimental and theoretical data mentioned in this article is available free of charge at http://pubs.acs.org.

Author Information

Corresponding Authors

*anderson@chem.utah.edu

*ana@chem.ucla.edu

Author Contributions: The project was conceived and planned in collaboration between all authors. Eric T. Baxter and Ashley C. Cass performed the experimental work and Mai-Anh Ha and Huanchen Zhai, the computational modeling. All authors contributed to the analysis of the results, and writing the manuscript.

Acknowledgments

This work was supported by the Air Force Office of Scientific Research under a Basic Research Initiative grant (AFOSR FA9550-16-1-0141) to A.N.A. and S.L.A. M.-A.H. was also funded by the UCLA Graduate Division Dissertation Year Fellowship. CPU resources at the DoD (Department of Defense) High Performance Computing Modernization Program (the US Air Force Research Laboratory DoD Supercomputing Resource Center—AFRL DSRC, the US Army Engineer Research and Development Center—ERDC, and the Navy Supercomputing Resource Center—Navy DSRC), Pacific Northwest National Laboratory's Environmental Molecular Sciences Laboratory's (EMSL) Cascade cluster, Extreme Science and Engineering Discovery

Environment’s (XSEDE) computing resources, and the UCLA-IDRE cluster were used to conduct this work.

References

1. Schulz, H. Short History and Present Trends of Fischer–Tropsch Synthesis. *Appl. Catal., A* **1999**, *186*, 3-12.

2. Rahimi, N.; Karimzadeh, R. Catalytic Cracking of Hydrocarbons over Modified Zsm-5 Zeolites to Produce Light Olefins: A Review. *Appl. Catal., A* **2011**, *398*, 1-17.

3. Shaikhutdinov, S. K.; Frank, M.; Bäumer, M.; Jackson, S. D.; Oldman, R. J.; Hemminger, J. C.; Freund, H.-J. Effect of Carbon Deposits on Reactivity of Supported Pd Model Catalysts. *Catal. Lett.* **2002**, *80*, 115-122.

4. Tan, K. F.; Chang, J.; Borgna, A.; Saeys, M. Effect of Boron Promotion on the Stability of Cobalt Fischer–Tropsch Catalysts. *J. Catal.* **2011**, *280*, 50-59.

5. Xu, J.; Chen, L.; Tan, K. F.; Borgna, A.; Saeys, M. Effect of Boron on the Stability of Ni Catalysts During Steam Methane Reforming. *J. Catal.* **2009**, *261*, 158-165.

6. Ha, M.-A.; Baxter, E. T.; Cass, A. C.; Anderson, S. L.; Alexandrova, A. N. Boron Switch for Selectivity of Catalytic Dehydrogenation on Size-Selected Pt Clusters on Al2o3. *J. Am. Chem. Soc.* **2017**, *139*, 11568-11575.

7. Rousset, J.; Cadrot, A.; Cadete Santos Aires, F.; Renouprez, A.; Mélinon, P.; Perez, A.; Pellarin, M.; Vialle, J.; Broyer, M. Study of Bimetallic Pd–Pt Clusters in Both Free and Supported Phases. *J. Chem. Phys.* **1995**, *102*, 8574-8585.

8. Yang, B.; Khadra, G.; Tuaillon-Combes, J.; Tyo, E. C.; Pellin, M. J.; Reinhart, B.; Seifert, S.; Chen, X.; Dupuis, V.; Vajda, S. Temperature-Dependent Evolution of the Oxidation States of Cobalt and Platinum in Co1–Xptx Clusters under H2 and Co + H2 Atmospheres. *J. Phys. Chem. C* **2016**, *120*, 21496-21504.

9. Bardotti, L.; Tournus, F.; Albin, C.; Boisron, O.; Dupuis, V. Self-Organisation of Size-Selected Coxpt1-X Clusters on Graphite. *Phys. Chem. Chem. Phys.* **2014**, *16*, 26653-26657.

10. Moskovkin, P.; Pisov, S.; Hou, M.; Raufast, C.; Tournus, F.; Favre, L.; Dupuis, V. Model Predictions and Experimental Characterization of Co-Pt Alloy Clusters. *Eur. Phys. J. D* **2007**, *43*, 27-32.

11. Kaden, W. E.; Kunkel, W. A.; Anderson, S. L. Cluster Size Effects on Sintering, Co Adsorption, and Implantation in Ir/Sio_2. *J. Chem. Phys.* **2009**, *131*, 114701, 1-15.

12. Roberts, F. S.; Kane, M. D.; Baxter, E. T.; Anderson, S. L. Oxygen Activation and Co Oxidation over Size-Selected Ptn/Alumina/Re(0001) Model Catalysts: Correlations with Valence Electronic Structure, Physical Structure, and Binding Sites. *Phys. Chem. Chem. Phys.* **2014**, *16*, 26443 – 26457.

13. Aizawa, M.; Lee, S.; Anderson, S. L. Deposition Dynamics and Chemical Properties of Size-Selected Ir Clusters on Tio2. *Surf. Sci.* **2003**, *542*, 253-275.

14. Baxter, E. T.; Ha, M.-A.; Cass, A. C.; Alexandrova, A. N.; Anderson, S. L. Ethylene Dehydrogenation on Pt4,7,8 Clusters on Al2o3: Strong Cluster Size Dependence Linked to Preferred Catalyst Morphologies. *ACS Catal.* **2017**, *7*, 3322-3335.

15. Blöchl, P. E. Projector Augmented-Wave Method. *Phys. Rev. B* **1994**, *50*, 17953.

16. Kresse, G.; Joubert, D. From Ultrasoft Pseudopotentials to the Projector Augmented-Wave Method. *Phys. Rev. B* **1999**, *59*, 1758.

17. Perdew, J. P.; Burke, K.; Ernzerhof, M. Generalized Gradient Approximation Made Simple. *Phys. Rev. lett.* **1996**, *77*, 3865.

18. Kresse, G.; Furthmüller, J. Efficient Iterative Schemes for Ab Initio Total-Energy Calculations Using a Plane-Wave Basis Set. *Phys. Rev. B* **1996**, *54*, 11169-86.

19. Kresse, G.; Furthmüller, J. Efficiency of Ab-Initio Total Energy Calculations for Metals and Semiconductors Using a Plane-Wave Basis Set. *Comput. Mater. Sci.* **1996**, *6*, 15-50.

20. Kresse, G.; Hafner, J. Ab Initio Molecular Dynamics for Liquid Metals. *Phys. Rev. B* **1993**, *47*, 558.

21. Kresse, G.; Hafner, J. Ab Initio Molecular-Dynamics Simulation of the Liquid-Metal–Amorphous-Semiconductor Transition in Germanium. *Phys. Rev. B* **1994**, *49*, 14251.

22. Bourdillon, A.; El-Mashri, S.; Forty, A. Application of Tem Extended Electron Energy Loss Fine Structure to the Study of Aluminium Oxide Films. *Philos. Mag. A* **1984**, *49*, 341-352.

23. Levin, I.; Brandon, D. Metastable Alumina Polymorphs: Crystal Structures and Transition Sequences. *J. Am. Ceram. Soc.* **1998**, *81*, 1995-2012.

24. Wales, D. J.; Doye, J. P. Global Optimization by Basin-Hopping and the Lowest Energy Structures of Lennard-Jones Clusters Containing up to 110 Atoms. *J. Phys. Chem. A* **1997**, *101*, 5111-5116.

25. Boyd, K. J.; Lapicki, A.; Aizawa, M.; Anderson, S. L. A Phase-Space-Compressing, Mass-Selecting Beamline for Hyperthermal, Focused Ion Beam Deposition. *Rev. Sci. Instrum.* **1998**, *69*, 4106-4115.

26. Kane, M. D.; Roberts, F. S.; Anderson, S. L. Mass-Selected Supported Cluster Catalysts: Size Effects on Co Oxidation Activity, Electronic Structure, and Thermal

Stability of Pd_n/Alumina (N ≤ 30) Model Catalysts. *Int. J. Mass Spectrom.* **2014**, *370*, 1-15.

27. Kane, M. D.; Roberts, F. S.; Anderson, S. L. Effects of Alumina Thickness on Co Oxidation Activity over Pd_{20}/Alumina/Re(0001): Correlated Effects of Alumina Electronic Properties and Pd_{20} Geometry on Activity. *J. Phys. Chem. C* **2015**, *119*, 1359–1375.

28. Chen, P. J.; Goodman, D. W. Epitaxial Growth of Ultrathin Al_2o_3 Films on Ta(110). *Surf. Sci.* **1994**, *312*, L767-L773.

29. Street, S. C.; Goodman, D. W. Chemical and Spectroscopic Studies of Ultrathin Oxide Films. *Chem. Phys. Solid Surf.* **1997**, *8*, 375-406.

30. Lai, X.; Chusuei, C. C.; Luo, K.; Guo, Q.; Goodman, D. W. Imaging Ultrathin Al2o3 Films with Scanning Tunneling Microscopy. *Chem. Phys. Lett.* **2000**, *330*, 226-230.

31. Wu, Y.; Garfunkel, E.; Madey, T. E. Growth and Oxidation of Ultra-Thin Al Films on the Re(0001) Surface. *Surf. Sci.* **1996**, *365*, 337-352.

32. Wu, Y.; Garfunkel, E.; Madey, T. E. Growth of Ultrathin Crystalline Al2o3 Films on Ru(0001) and Re(0001) Surfaces. *J. Vac. Sci. Technol., A* **1996**, *14*, 2554-2563.

33. Yu, J.; Boatz, J. A.; Anderson, S. L. Borane-Aluminum Surface Interactions: Enhanced Fracturing and Generation of Boron-Aluminum Core-Shell Nanoparticles. *J. Phys. Chem. C* **2017**, *121*, 14176-14190.

34. Yeh, J. J.; Lindau, I. Atomic Subshell Photoionization Cross Sections and Asymmetry Parameters: 1< Z < 103. *At. Data and Nucl. Data Tables* **1985**, *32*, 1-155.

35. Rabalais, J. W. *Principles and Applications of Ion Scattering Spectrometry : Surface Chemical and Structural Analysis*; Wiley: New York, 2003; pp 336.

36. Bandiera, J.; Naccache, C.; Mathieu, M. V. Products Formed by the Hydrolysis of Diborane in Contact with Γ-Alumina. *C. R. Acad. Sci., Paris, Ser. C* **1969**, *268*, 901-4.

37. Stein, S. E., director Ir and Mass Spectra. In *Nist Chemistry Webbook, Nist Standard Reference Database Number 69*, Mallard, W. G.; Linstrom, P. J., Eds. NIST Mass Spec Data Center, National Institute of Standards and Technology: Gaithersburg MD 20899 (http://webbook.nist.gov). 2000.

38. Chase, M. W., Jr. ; Davies, C. A.; Downey, J. R., Jr.; Frurip, D. J.; McDonald, R. A. Janaf Thermochemical Tables, Third Edition. *J. Phys. Chem. Ref. Data* **1985**, *14*

39. Fehlner, T. P.; Koski, W. S. Direct Detection of the Borane Molecule and the Boryl Radical by Mass Spectrometry. *J. Am. Chem. Soc.* **1964**, *86*, 2733-2734.

40. Kaden, W. E.; Kunkel, W. A.; Roberts, F. S.; Kane, M.; Anderson, S. L. Co Adsorption and Desorption on Size-Selected Pdn/Tio2(110) Model Catalysts: Size Dependence of Binding Sites and Energies, and Support-Mediated Adsorption. *J. Chem. Phys.* **2012**, *136*, 204705/1-204705/12.

41. Zhai, H.; Alexandrova, A. N. Fluxionality of Catalytic Clusters: When It Matters and How to Address It. *ACS Catal.* **2017**, *7*, 1905-1911.

42. Gao, M.; Lyalin, A.; Takagi, M.; Maeda, S.; Taketsugu, T. Reactivity of Gold Clusters in the Regime of Structural Fluxionality. *J. Phys. Chem. C* **2015**, *119*, 11120-11130.

43. Hakkinen, H.; Abbet, S.; Sanchez, A.; Heiz, U.; Landman, U. Structural, Electronic, and Impurity-Doping Effects in Nanoscale Chemistry: Supported Gold Nanoclusters. *Angew. Chem., Int. Ed.* **2003**, *42*, 1297-1300.

44. Xing, X.; Li, X.; Yoon, B.; Landman, U.; Parks, J. H. Dynamic Fluxionality and Enhanced Co Adsorption in the Presence of Coadsorbed H 2 O on Free Gold Cluster Cations. *Int. J. Mass Spectrom.* **2015**, *377*, 393-402.

45. Sams, R. L.; Blake, T. A.; Sharpe, S. W.; Flaud, J. M.; Lafferty, W. J. High-Resolution Infrared Study of the N14, N17, and N18bands Of11b2h6and10b11bh6. *J. Mol. Spectrosc.* **1998**, *191*, 331-342.

46. Huynh, M. T.; Alexandrova, A. N. Persistent Covalency and Planarity in the B N Al6–N 2–and Lib N Al6–N–(N= 0–6) Cluster Ions. *J. Phys. Chem. Lett.* **2011**, *2*, 2046-2051.

47. Dadras, J.; Jimenez-Izal, E.; Alexandrova, A. N. Alloying Pt Sub-Nano-Clusters with Boron: Sintering Preventative and Coke Antagonist? *ACS Catal.* **2015**, 5719-5727.

48. Perry, D. A.; Hemminger, J. C. Σ-Bond Metathesis on a Surface: Dehydrogenation of Cyclohexane on Hydrogen-Saturated Pt (111). *J. Am. Chem. Soc.* **2000**, *122*, 8079-8080.

49. Carlsson, A.; Madix, R. The Dynamics of Ethylene Adsorption on Pt (111) into Di-Σ and Π-Bonded States. *J. Chem. Phys.* **2001**, *115*, 8074-8082.

50. Stöhr, J.; Sette, F.; Johnson, A. L. Near-Edge X-Ray-Absorption Fine-Structure Studies of Chemisorbed Hydrocarbons: Bond Lengths with a Ruler. *Phys. Rev. Lett.* **1984**, *53*, 1684.

51. Ha, M.-A.; Dadras, J.; Alexandrova, A. Rutile-Deposited Pt–Pd Clusters: A Hypothesis Regarding the Stability at 50/50 Ratio. *ACS Catal.* **2014**, *4*, 3570-3580.

52. Moulder, J. F.; Stickle, W. F.; Sobol, P. E.; Bomben, K. D.; J. Chastain & R. C. King, J., eds. *Handbook of X-Ray Photoelectron Spectroscopy*; Physical Electronics: Eden Prarie, MN, 1995.

53. Powell, C. J.; Jablonski, A. *Nist Electron Effective-Attenuation-Length Database* 1.0; NIST: Gaithersburg, 2001.

54. Briggs, D.; Seah, M. P. *Practical Surface Analysis, Volume 1 : Auger and X-Ray Photoelectron Spectroscopy,* , 2nd ed.; John Wiley & sons: Chichester, 1992; Vol. 1; pp 1-657.

55. Wagner, C. D.; Naumkin, A. V.; Kraut-Vass, A.; Allison, J. W.; Powell, C. J.; Jr., J. R. R. Nist X-Ray Photoelectron Spectroscopy Database. *NIST Standard Reference Database 20, Version 3.2 (Web Version)* **2000**.

56. Pasquale, F. L.; Kelber, J. A. Site-Specific Electron-Induced Cross-Linking of Ortho-Carborane to Form Semiconducting Boron Carbide. *Appl. Surf. Sci.* **2012**, *258*, 2639-2642.

TOC Graphic